Research Article **Open Access**

Laurent Olislager, Wakana Kubo, Takuo Tanaka, Simona Ungureanu, Renaud A. L. Vallée, Branko Kolaric*, Philippe Emplit, and Serge Massar

Propagation and survival of frequency-bin entangled photons in metallic nanostructures

DOI 10.1515/nanoph-2015-0011
Received February 6, 2015; accepted May 2, 2015

Abstract: We report on the design of two plasmonic nanostructures and the propagation of frequency-bin entangled photons through them. The experimental findings clearly show the robustness of frequency-bin entanglement, which survives after interactions with both a hybrid plasmo-photonic structure, and a nano-pillar array. These results confirm that quantum states can be encoded into the collective motion of a many-body electronic system without demolishing their quantum nature, and pave the way towards applications of plasmonic structures in quantum information.

PACS: 42.50.Dv, 03.67.Mn, 73.20.Mf, 71.36.+c

1 Introduction

Surface plasmon polaritons (SPPs) are virtual particles resulting from the coupling of light to the collective oscillation of the conduction electrons at a metal-dielectric interface. Due to the evanescent field in the direction perpendicular to its propagation, a SPP generates a strong confinement of the incident light at the interface. Moreover, reports have shown that plasmons maintain non-classical photon statistics, and preserve entanglement, allowing for the encoding of entangled photons in multi-electronic systems.

Recently, the interest for quantum plasmonics has increased in the physics community, in view of its unique capabilities to control and manipulate non-classical states of light by using plasmonic resonances. Integrated quantum technologies based on SPPs or localized surface plasmon polaritons (LSPPs) hold great potential for various applications in quantum information processing, since it allows scalability and miniaturization as well as a coherent coupling to single emitters [1–3]. Additionally, control and manipulation of quantum light using light-matter interactions at the nanoscale could lead to new classes of quantum devices, such as single-photon sources, transistors and ultra-compact circuitry, with potential applications for secure communication and advanced computing [4–6]. Plasmonic excitations have recently emerged as an interesting carrier of quantum information.

Beyond interest for potential applications, a lot of studies have focused on fundamental issues. Of particular interest is the exploration of the so-called mesoscopic world, in which quantum states are coherently carried by billions of electrons. Recent works include single-particle experiments, such as Young's double-slit experiment [7], other demonstrations of quantum superpositions of single plasmons [8–12], the generation of plasmonic squeezed states [13], and double-particle experiments [14–19], such as demonstration of the Hong-Ou-Mandel effect with plasmons, directly demonstrating the quantum bosonic nature of plasmonic excitations.

We focus on studies involving entanglement. Metallic nanostructures allow conversion of photons into surface plasmons which tunnel through the structure before reradiating as photons [20, 21]. This photon-plasmon-photon conversion has been investigated with polarization [22] (see also the theoretical analysis of [23]), time-bin [24] and orbital angular-momentum [25] entanglement. In these works, the plasmonic structures consisted of two dimen-

Laurent Olislager, Philippe Emplit: OPERA–Photonique, CP 194/5, Université libre de Bruxelles, av. F.D. Roosevelt 50, Brussels B-1050, Belgium, E-mail: lolislag@ulb.ac.be
Wakana Kubo, Takuo Tanaka: RIKEN, Metamaterials Laboratory 2-1 Hirosawa, Wako, Saitama, Japan.
Simona Ungureanu, Renaud A. L. Vallée: CNRS, University Bordeaux, CRPP, UPR 8641, 115 av. Schweitzer, Pessac F-33600, France
***Corresponding Author: Branko Kolaric:** Laboratoire Interfaces and Fluides Complexes, Centre d'Innovation et de Recherche en Materiaux Polymeres, University of Mons, 20 Place du Parc, B-7000 Mons, Belgium and Research Center in Physics of Matter and Radiation (PMR), Department of Physics, University of Namur, 61 rue de Bruxelles, B-5000 Namur, Belgium, E-mail: branko.kolaric@unamur.be
Serge Massar: Laboratoire d'Information Quantique, CP 225, Université libre de Bruxelles, av. F.D. Roosevelt 50, Brussels B-1050, Belgium

sional hole arrays [22, 24, 25] and long range surface plasmon polaritons [24]. The investigated wavelengths were 813 nm [22], 810 nm and 1550 nm [24], 702 nm [25]. In all cases, there was no unexplained decrease in the visiblities of two-photon interference fringes, with observed visibilities of 96% or higher.

Frequency-bin entanglement has recently emerged as a good alternative degree of freedom for quantum optics experiments. Manipulating energy-time entangled photons directly in the frequency domain allows robust transmission through telecommunication fibers, high-visibility two-photon interference and violation of Bell inequalities [26–28]. Here we present an analysis of interactions of frequency-bin entangled photons with different plasmo-photonic nanostructures. Specifically, in this study we address two pivotal questions. First, in which cases and to what extent does frequency-bin entanglement survive when a photon is subject to a plasmonic conversion? Second, could the nature of a resonance affect the coherence of the photon–plasmon–photon conversion process?

Concerning the second aspect, we investigated two structures. The first is a hybrid plasmo-photonic structure (HPPS) made by nanosphere lithography. This HPPS was designed by combining a continuous metal film and a dielectric photonic crystal. It presents a rich resonance pattern [29, 30] and supports both SPPs and LSPPs, allowing to control the interplay between them and their eventual mixing. The second structure consists of a gold nano-pillar arrays (NPAs) fabricated by nanocoating lithography [31–33].

We analyzed the propagation of frequency-bin entangled photons through these two structures, taking care that the optical frequencies are matched with the plasmo-photonic resonances, thereby allowing us to investigate whether these structures affect the photon–plasmon–photon conversion processes.

In our experiment, the frequency of the entangled photons was 1552 nm. Net visibilities after passing through the samples are in the range of 95–98%. We did not find any evidence that frequency-bin entanglement is affected by the photon–plasmon–photon conversion. Our results thus confirm that there are no unexpected decoherence effects in the investigated mesoscopic regime, and that a wide range of plasmonic structures can be used for quantum information processing.

2 Materials and methods

Fabrication of hybrid plasmo-photonic structures and gold nano-pillar arrays

The HPPS was fabricated by the nanosphere lithography technique previously reported in [29, 30]. Latex micro-spheres [diameters D = 1 μm, 2.5% (weight to volume fraction) solids aqueous suspensions] were supplied by Polysciences. Gold (99.999%, 3 × 6 mm^2) was purchased from Neyco. Glass plates with a size of 2×2 cm^2 and a thickness of 5 mm were carefully cleaned and treated with UV-ozone for 30 minutes. An opportune ratio of Triton (10^{-3} in mass) dispersed in a solution containing water and the polystyrene micro-spheres were then deposited on the glass surface and dried under a tilt angle of approximately 10 degrees under controlled conditions of temperature and humidity (T = 293 K, H = 65%). These conditions led to the formation of large areas of latex micro-spheres mono-layers well-ordered in a closely packed hexagonal array [29, 30]. The structure was then covered with 50 nm of gold by using a Boc-Edwards Auto306 evaporator. The thickness was controlled by an *in-situ* mounted quartz crystal micro-balance.

NPAs were fabricated by the nanocoating lithography technique, as previously reported in [31–33]. We used as substrate either a transparent polymer film (Zeon Corporation, ZeonorFilm ®, ZF-14) or a glass substrate covered by a polymer film. The thickness of the polymer film substrate is 100 μm, its refractive index at sodium D line is 1.53, and total light transmittance is 92%. In the case of the glass substrate, a polymer solution (Maruzen Petrochemical, COC solution) was coated on the substrate by spin-coating, resulting in a polymer film of 1 μm thickness. The film on a glass plate showed similar optical characteristics as the polymer film. A pillar-shaped polymer template was realized by imprinting on the flexible transparent polymer film or on the polymer film on the glass plate. The pillar width and height were 200 nm and the pitch between each nano-pillar was 460 nm. The pillar-shape templates formed an hexagonal structure. In our experiments, we used the sample with a glass substrate.

A gold layer of 50 nm thickness was deposited on the template by sputtering (Sanyu Electron, SC-701MC). The gold-covered template was subjected to reactive ion etching treatment. Reactive ion etching treatment is an anisotropic dry etching process that removes the gold layer only on the top and bottom surfaces of the template (Samco, RIE-200NL, power 100 W, pressure 5 Pa, treatment time 4 minutes). This process left only side-wall layers,

leading to the formation of gold nano-pillars. Finally, the sample was subjected to O_2 plasma treatment to remove the polymer template, resulting in arrays of hollow gold nano-pillars.

Spectral measurements and simulations

The transmission (T) and reflection (R) spectra of the HPPS and NPA were measured at normal incidence with the 20/20 PV dual microspectrophotometer from CRAIC Technologies, on sample areas of $100 \times 100\ \mu m^2$. The normalization of the spectra was performed with respect to the glass substrate. The reflection spectra were also measured at various incidence angles with respect to the sample's normal, using a Lambda 950 Perkin Elmer UV/VIS/NIR spectrometer equipped with the Universal Reflectance Accessory. The absorption (A) spectra were deduced from the relation $A = 1 - R - T$.

The T, R, A spectra of both types of structures were simulated by solving Maxwell's equations using the three-dimensional finite-difference time-domain method, implemented in the freely available MEEP software package [34]. By Fourier transforming the response to a short, broadband, spatially extended gaussian pulse in the far-field of the structures and normalizing with the response of a reference (the glass substrate) for the same excitation conditions, a single simulation yielded the T, R, A spectra over a wide spectrum of frequencies. The electrical near-field patterns of the plasmo-photonic structures were obtained by sending a narrow-band, frequency-gated, and spatially-extended Gaussian pulse in the far-field of the structure and recording the three components of the electric field in time. In all types of simulations, the wave-vector is normal to either the substrate or the sample's surface. Periodic boundary conditions were implemented laterally, and perfectly matched layers were implemented longitudinally, in the propagation direction. The dielectric permittivities of the glass substrate and the polystyrene spheres were taken to be 2.3 and 2.5, respectively. The dielectric permittivity of gold was specified by using a sum of Drude and Drude–Lorentz terms, following Rakic et al. [35]

Measurement of frequency-bin entanglement

Spontaneous parametric down-conversion occurs when a monochromatic laser pumps a second-order nonlinear crystal: a pump photon at (angular) frequency ω_p creates two daughter photons, denoted signal (s) and idler (i) photons. Conservation of energy implies that $\omega_s + \omega_i = \omega_p$: the sum of the frequencies of the signal and idler photons is determined but the frequency of each photon is uncertain. The bi-photon state is thus frequency-entangled, and can be idealized as:

$$|\Psi\rangle = \int \mathrm{d}\omega\ |\omega_0 + \omega\rangle_\mathrm{A}\, |\omega_0 - \omega\rangle_\mathrm{B}\ , \tag{1}$$

where $|\omega\rangle$ represents a single photon at frequency ω, and A and B denote that the signal and idler photons are sent to different protagonists, commonly called Alice and Bob.

The quantum optics experiment follows closely that reported in [28] (except for the frequency filters that are of the type used in [27]). In detail, a continuous-wave laser (from Sacher Lasertechnik) with wavelength $\lambda_p = 2\pi c/\omega_p = 776.04$ nm pumps a periodically-poled lithium niobate waveguide (from HC Photonics), thus generating frequency-entangled photons around wavelength $\lambda_0 = 2\pi c/\omega_0 = 1552.08$ nm. The bandwidth of the photons extends on the whole telecommunication C-band. The photons are separated with an optical coupler and sent through standard optical fibers. In the present experiment, photon B is coupled out of its fiber, transmitted through a plasmonic nanostructure, and re-coupled into a fiber. The spot size on the plasmonic structure is a few square millimeter, much larger than the nanostructures.

Figure 1 schematically depicts our experiment.

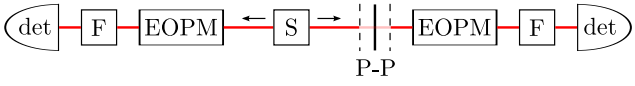

Figure 1: Experimental setup for generating frequency-entangled photons (source S) and measuring two-photon interference in the frequency domain (electro-optic phase modulators EOPMs, frequency filters F, single-photon detectors det) after a photon has been subject to a photon–plasmon–photon conversion (P-P). See text for a detailed description.

Each photon passes through a different fiber-pigtailed electro-optic phase modulator (from EOspace) driven by a radio-frequency signal $V(t) = v\sin(\varphi - \Omega t)$, with adjustable amplitude v and phase φ. Due to the electro-optic effect, a photon's frequency state is transformed according to:

$$\hat{U}(c, \varphi)\,|\omega\rangle = \sum_n J_n(c) e^{in\varphi}\,|\omega + n\Omega\rangle\ , \tag{2}$$

with J_n a Bessel function of the first kind, $c = \pi v/V_\pi$, and V_π characteristic of the modulator's response. A phase modulator therefore creates frequency sidebands separated by the modulation frequency, which corresponds to a quantum superposition of frequency bins.

Photons A and B are modulated at the same radio-frequency $\Omega/2\pi = 25$ GHz, but with adjustable amplitudes and phases, (a, α) for photon A and (b, β) for photon B. These parameters are set independently and precisely with a dedicated radio-frequency architecture based on remotely controlled phase shifters and attenuators. Using (1) and (2), the joint probability to detect photon B at frequency ω_0 given that photon A is detected at frequency ω_0 (and conversely) reads

$$P = J_0^2\left\{[a^2 + b^2 + 2ab\cos(\alpha - \beta - \phi_0)]^{1/2}\right\}. \quad (3)$$

In this equation, we have added a phase offset ϕ_0 that corresponds to the RF phase acquired by photons and RF signals traveling from the photon pair source and the RF source, respectively. This offset phase has to be determined experimentally, but is fixed throughout the duration of the experiment.

Note that $P = 1$ when $a = b = 0$, as expected by energy conservation. With phase modulation, P is a function of a global parameter depending on (a, α) and (b, β). This is a signature of a non-local two-photon interference in the frequency domain, signature of the frequency entanglement allowing Bell inequality violations. Note that individual probabilities to detect each photon at a given frequency ω_A or ω_B are not affected by the modulation.

Such an interference pattern can be detected with narrow-band frequency filters and single-photon detectors. In our experiment, each electro-optic phase modulator is followed by a fiber Bragg grating (from Acreo) aligned on frequency ω_0. The spectral characteristics of the filter (full-width-at-half-maximum $\approx$ 4 GHz and isolation at 12.5 GHz $\approx$ 30 dB) allow a correct discrimination of the frequency bins. Photons belonging to the frequency bin centered on ω_0 are sent to avalanche photodiodes (from id Quantique) operated in gated mode. Detection efficiency is 10%, gate width is 100 ns, repetition rate is 100 kHz, and dark-count rate $\approx$ 200 Hz.

A time-to-digital converter (Agilent Acqiris) records the time delays between events common to Alice's and Bob's detectors. A histogram of these events reveals a coincidence peak when correlated photons are present. Taking into account noise, the (net) number of events in this peak is supposedly proportional to the joint probability detection: $N \propto P$. In the present experiment, we chose radio-frequency amplitudes $a \approx b \approx 1.2$ and a fixed radio-frequency phase β, and we varied α between 0 and 2π. In this case, P should be maximal (and equal to 1) when $\alpha - \beta - \phi_0 = \pi$, and minimal (and equal to 0) when $2a^2[1 + \cos(\alpha - \beta - \phi_0)]$ is a root of J_0, see (3). This procedure thus allows the evaluation of the visibility of the two-photon interference pattern:

$$V = \frac{N_{\max} - N_{\min}}{N_{\max} + N_{\min}}, \quad (4)$$

with $N_{\max}$ ($N_{\min}$) corresponding to the maximal (minimal) number of counts registered in the coincidence peak. Net values are obtained from raw values by removing the contribution of accidental coincidences, evaluated from the background noise in the histogram.

3 Resonances of plasmo-photonic nanostructures

In order to characterize the resonance patterns of the HPPS (a mono-layer of hexagonal close packed polystyrene beads of diameter $D = 1000$ nm covered with 50 nm of gold) and the NPA (a hexagonal array with pitch 460 nm of cylindrical gold pillars of width and height 200 nm, thickness 50 nm), we measured their T, R, A spectra.

The measured spectra of the HPPS are given in figure 2 (left panel). The optical transmission spectrum of the HPPS is significantly structured. On the contrary, a flat gold film would exhibit the well-known featureless spectrum of a semi-transparent film, being rather opaque in the visible range [29]. Accordingly, the overall transmission of the HPPS is strongly increased compared to the transmission of a flat continuous metallic film of the same nominal thickness. It exhibits well-defined maxima and minima, with an asymmetric peak that resembles very much the one previously reported for extraordinary transmission of metallic subwavelength hole arrays [22]. The major asymmetric peak is observed around 1300 nm and is attributed to a Bragg-plasmon mode [29], resulting from the periodicity of the structure and the commensurability of the lattices at the metal-dielectric interface. On the long-wavelength side of this peak, a significantly reduced transmission is observed, which also corresponds to a maximum of absorption. This feature, centered at 1600 nm, can be confidentially assigned to a LSPP mode. In order to better match the resonance frequency of the Bragg-plasmon mode with the frequency-entangled photons, we shifted the incidence angle to $\pi/4$. According to the Bragg-plasmon law [30], this shifts the transmission maximum to:

$$\lambda = \frac{\sqrt{3}D}{2}\sqrt{\epsilon_{\text{eff}}(\lambda) + \sin^2\theta}, \quad (5)$$

where ϵ_{eff} is the effective permittivity expressed by the plasmonic-dielectric interface mixing rule $1/\epsilon_{\text{eff}}(\lambda) = 1/\epsilon_{\text{gold}}(\lambda) + 1/\epsilon_{\text{dielectric}}(\lambda)$, $\epsilon_{\text{dielectric}}$ being defined on a filling factor basis, $\epsilon_{\text{dielectric}} = \epsilon_{\text{polystyrene}} f + \epsilon_{\text{air}}(1 - f)$.

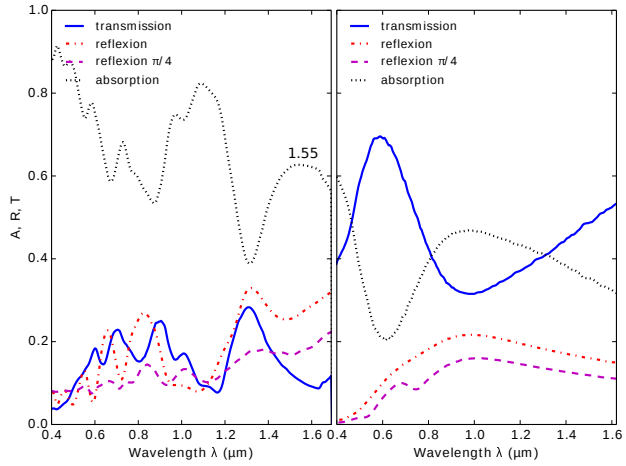

Figure 2: *Experiments.* Transmission (T, blue solid line), reflection (R, red dashed-dotted line) and absorption (A, black dotted line) spectra of the HPPS (left, the absorption maxima are at 1.1 μm and 1.55 μm) and NPA (right, absorption maximum at 1 μm) measured at normal incidence. The magenta dashed lines are the reflection spectra taken at an incidence angle $\theta = \pi/4$ with respect to the sample's normal.

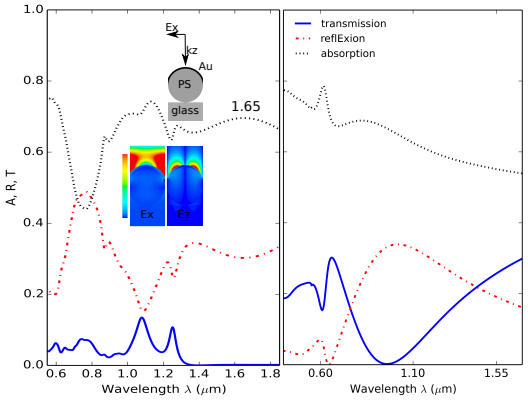

Figure 3: *Simulations.* Transmission (T, blue solid line), reflection (R, red dashed-dotted line) and absorption (A, black dotted line) spectra of the HPPS (left, absorption maxima are at 1.1 μm and 1.65 μm) and NPA (right, note the absorption maximum at 1 μm). The insets show a cut in the xz plane of the geometry (in gray–black) of the HPPS and the E_x and E_z near-field patterns (in color) at the wavelength of the incident entangled photons ($\lambda = 1.552$ μm). Light is polarized along the x axis and propagates along the z axis. The color scales from blue (minimum intensity) to red (maximum intensity).

The simulated spectra of the HPPS are given in figure 3 (left panel). They are in good agreement with the measured spectra.In particular, a transmission maximum at 1300 nm, corresponding to an absorption minimum, is recovered, signaling the Bragg-plasmon mode. Furthermore, a broad absorption peak, corresponding to a minimum transmission, and centered at 1600 nm, is also found, as a characteristic of the LSPP resonance. The near-field intensity pattern at the wavelength of the frequency-entangled photons ($\lambda = 1.552$ μm) propagating through the structure is shown in the inset of figure 3. The E_x field intensity does not penetrate the glass substrate (bottom) and, instead, shows a strong confinement on the air–metal interface (top of the figure). The E_z intensity map is also largely confined to the air–metal interface, the field intensity propagating only slightly in the sphere. These features correspond nicely with the existence of an LSPP mode at this wavelength. However, the small difference in optical response between simulated and experimentally obtained data is due to the fact, that the simulated optical response are calculated assuming the perfect defect free structure/array.

We also performed similar spectral measurements and simulations on the Au NPA, see right panels of figures 2 and 3. The optical properties of metallic nanoparticles are influenced by particle size, shape, environment and, possibly (i.e. if close enough) by their mutual orientations. The minimum transmission exhibited at around 1 μm, that coincides with an absorption maximum, suggests the occurence of an LSPP resonance. This absorption peak is rather broad. One might think, at first glance, that the large width could be due to a disordered arrangement of the pillars in the array, or to the pillars varying slightly in size or shape. However, exactly the same feature appear in the spectrum obtained from finite difference time-domain simulations based on an idealized arrangement of ideally sized and shaped pillars, precluding the attribution of the large peak to some imperfections of the NPA. The width of the peak is therefore probably due to a large radiative damping of the plasmon mode involved. This peak extends significantly to the wavelength ($\lambda = 1.552$ μm) at which the propagation and survival of the frequency-bin entangled photons is investigated.

For all structures, the measured optical losses at the wavelength $\lambda = 1.552$ μm are sufficiently low, see table 1, to allow a detailed study in the quantum regime.

4 Quantum study

We first investigated whether frequency-bin entanglement was preserved when one of the two photons of an entangled pair is transferred through our plasmonic nanostructures. In order to perform this observation, we followed experimental procedures similar to those used in previous works [22, 24, 25].

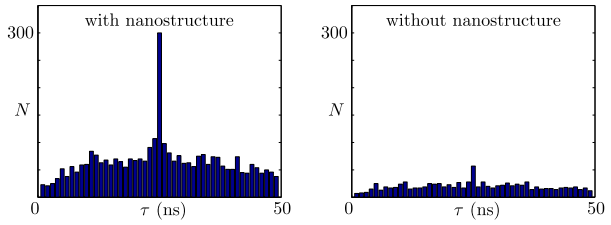

Figure 4: *Coincidence peaks.* Coincidence peaks obtained after one photon of the entangled pair is transferred through either the HPPS at normal incidence (left) or a flat gold film (right).

Table 1: *Summary of results.* We quote the loss of each sample (measured with classical light), the rate of coincident detection for entangled photons (when phase modulation is off), and the visibility V of the two-photon interference pattern (extracted from coincidence measurements when phase modulation is on, see fig. 5 and eq. 4). In the case of a flat gold film, losses where too high to obtain reliable visibilities.

sample	loss (dB)	rate (Hz)	V (%)
HPPS at 0 degrees	10	0.50 ± 0.10	96 ± 2
HPPS at 45 degrees	16	0.10 ± 0.04	98 ± 2
flat gold film	21	0.05 ± 0.02	—
NPA	6	0.75 ± 0.10	95 ± 2
no sample	0	3 ± 1	98 ± 2

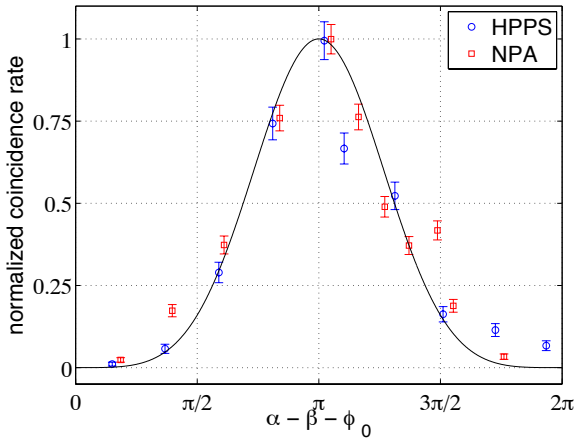

Figure 5: *Two-photon interference pattern.* Two-photon interferences obtained after photon–plasmon–photon conversion of one photon of the entangled pair through the HPPS or NPA. Symbols represent the experimental measurements. Vertical axis is the normalized net coincidence rate, i.e. the coincidence rate divided by the coincidence rate when modulation is off, with accidental coincidences subtracted. Statistical error bars are indicated. The horizontal axis is the phase $\alpha - \beta - \phi_0$, when the phase α of Alice's modulator is scanned, and when β and ϕ_0 are kept fixed. The RF amplitudes where adjusted to the values $a \approx b \approx 1.2$ in which case the coincidence curve has a single zero when $\alpha - \beta - \phi_0 = 0$ The continuous curve represents the theoretical predictions. The only adjustable parameter when fitting the theoretical prediction is the phase ϕ_0 which is unknown.

Figure 4 shows typical results performed on our structures. Results shown in the left (right) panels pertain either to the HPPS (50 nm gold deposited on nanosphere array) or to a 50-nm gold layer deposited on a glass substrate. Similar results were obtained for the NPA. When the HPPS was used at an angle of 45 degrees, the photon frequency matches with the Bragg plasmon mode, causing slight increase of the measured coincidence rates (typically of the order of Hz) that are consistent with the measured loss values. Note that coincidences are almost fully lost in the case of non-structured film, due to its much higher loss. The measured coincidence rates (typically of the order of Hz) are consistent with the loss values given in table 1.They were measured by using the same setup as for the quantum measurements (see Figure 1). But a classical light source was used, and the power transmitted through the setup was measured, referenced to the case where the sample was absent. Since all samples were characterized using the same setup (the incident light had approximately the same spatial properties), the measured values for losses are fully reproducible and are closely correlated to the structure of the sample. The enhanced coincidence peak and signal-to-noise ratio on the left panel of Figure 4 clearly highlights the role of the plasmonic resonance. The enhanced coincidence peak and signal-to-noise ratio on the left panel clearly highlights the role of the plasmonic resonance on the survival of photons, and hence entanglement, when they pass through the HPPS, as the vast majority of analyzed photons have indeed been subject to a photon–plasmon–photon conversion.

Furthermore, we confirmed that entanglement is preserved after photon-plasmon-photon conversion by varying the phase α of Alice's modulator. Figure 5 shows the resulting two-photon interference pattern. The continuous curve is the theoretical prediction eq. (3). Experimental measurements —extracted from coincidence peaks such as the ones of figure 4— are in good agreement with the predictions. After subtraction of the background noise, large net visibilities are obtained, see table 1. As shown in [26–28], frequency-bin entanglement can be used to violate the Clauser–Horne Bell inequality, by a theoretical maximal value of $S = 2.389$. Measured visibilities should allow a violation of at least 2.2.

5 Conclusion

In the present work, we have studied the preservation of entanglement during photon–plasmon–photon conversion. For both the plasmonic structures investigated, a nanosphere array and a nanopillar array, and the type of entanglement used, frequency-bin entanglement, had not been studied previously in this context. We find no evidence for decrease of coherence when photons are converted to mesoscopic electronic excitations. Indeed, the only parameter that seems to influence the results are the losses of the samples, which are much higher for a flat gold film than for the investigated plasmonic structures due to the existence of plasmonic resonances.

Our experiment can be the basis for further studies on the link between the nature of plasmonic resonances and the photon-plasmon-photon conversion processes. It may also contribute to the development of applications of metallic nanostructures in quantum-based technologies.

Acknowledgement: This research was supported by the Interuniversity Attraction Poles program of the Belgian Science Policy Office, under the grant IAP P7-35 photonics@be, by the F.R.S.-FNRS, and by the Région Aquitaine (France). L. O. acknowledges financial support from the Fonds David et Alice Van Buuren. B. K. acknowledges financial support from the Smart film grant 830039 in the framework of Convergence Project of the Region Wallonne and action de Recherche Concertee (BIOSTRUCT project) of the University of Namur (Unamur). BK additionally acknowledges the support from the Nanoscale Quantum Optics COST-MP1403 action.

References

[1] Zubin Jacob and Vladimir Shalaev. Plasmonics goes quantum. 2011.

[2] Zubin Jacob. Quantum plasmonics. *Mrs Bull.*, 37(08):761–767, 2012.

[3] M S Tame, K R McEnery, S K Özdemir, J Lee, S A Maier, and M S Kim. Quantum plasmonics. *Nat. Phys.*, 9(6):329–340, 2013.

[4] Michael A Nielsen and Isaac L Chuang. *Quantum computation and quantum information*. Cambridge university press, 2010.

[5] Igor Aharonovich, Andrew D Greentree, and Steven Prawer. Diamond photonics. *Nat. Photonics*, 5(7):397–405, 2011.

[6] Alexander Huck, Shailesh Kumar, Abdul Shakoor, and Ulrik L Andersen. Controlled coupling of a single nitrogen-vacancy center to a silver nanowire. *Phys. Rev. Lett.*, 106(9):96801, 2011.

[7] H F Schouten, N Kuzmin, G Dubois, T D Visser, G Gbur, P F A Alkemade, H Blok, D Lenstra, E R Eliel, and Others. Plasmon-assisted two-slit transmission: Young's experiment revisited. *Phys. Rev. Lett.*, 94(5):53901, 2005.

[8] Sylvain Fasel, Matthäus Halder, Nicolas Gisin, and Hugo Zbinden. Quantum superposition and entanglement of mesoscopic plasmons. *New J. Phys.*, 8(1):13, 2006.

[9] A V Akimov, A Mukherjee, C L Yu, D E Chang, A S Zibrov, P R Hemmer, H Park, and M D Lukin. Generation of single optical plasmons in metallic nanowires coupled to quantum dots. *Nature*, 450(7168):402–406, 2007.

[10] Roman Kolesov, Bernhard Grotz, Gopalakrishnan Balasubramanian, Rainer J Stöhr, Aurélien A L Nicolet, Philip R Hemmer, Fedor Jelezko, and Jörg Wrachtrup. Wave–particle duality of single surface plasmon polaritons. *Nat. Phys.*, 5(7):470–474, 2009.

[11] Giuliana Di Martino, Yannick Sonnefraud, Stéphane Kéna-Cohen, Mark Tame, Sahin K Özdemir, M S Kim, and Stefan A Maier. Quantum statistics of surface plasmon polaritons in metallic stripe waveguides. *Nano Lett.*, 12(5):2504–2508, 2012.

[12] Yong-Jing Cai, Ming Li, Xi-Feng Ren, Chang-Ling Zou, Xiao Xiong, Hua-Lin Lei, Bi-Heng Liu, Guo-Ping Guo, and Guang-Can Guo. High visibility on-chip quantum interference of single surface plasmons. *arXiv Prepr. arXiv1402.0955*, 2014.

[13] Alexander Huck, Stephan Smolka, Peter Lodahl, Anders S Sø rensen, Alexandra Boltasseva, Jiri Janousek, and Ulrik L Andersen. Demonstration of quadrature-squeezed surface plasmons in a gold waveguide. *Phys. Rev. Lett.*, 102(24):246802, 2009.

[14] A Gonzalez-Tudela, Diego Martin-Cano, Esteban Moreno, Luis Martin-Moreno, C Tejedor, and Francisco J Garcia-Vidal. Entanglement of two qubits mediated by one-dimensional plasmonic waveguides. *Phys. Rev. Lett.*, 106(2):20501, 2011.

[15] Reinier W Heeres, Leo P Kouwenhoven, and Valery Zwiller. Quantum interference in plasmonic circuits. *Nat. Nanotechnol.*, 8(10):719–722, 2013.

[16] S Dutta Gupta and G S Agarwal. Two-photon quantum interference in plasmonics: theory and applications. *Opt. Lett.*, 39(2):390–393, 2014.

[17] James S Fakonas, Hyunseok Lee, Yousif A Kelaita, and Harry A Atwater. Two-plasmon quantum interference. *Nat. Photonics*, 8(4):317–320, 2014.

[18] Michael Steel. Quantum plasmonics: Two-plasmon interference. *Nat. Photonics*, 8(4):273–275, 2014.

[19] G Di Martino, Y Sonnefraud, M S Tame, S Kéna-Cohen, F Dieleman, \cSK Özdemir, M S Kim, and S A Maier. Observation of quantum interference in the plasmonic Hong-Ou-Mandel effect. *Phys. Rev. Appl.*, 1(3):34004, 2014.

[20] Thomas W Ebbesen, H J Lezec, H F Ghaemi, Tineke Thio, and P A Wolff. Extraordinary optical transmission through subwavelength hole arrays. *Nature*, 391(6668):667–669, 1998.

[21] L Martin-Moreno, F J Garcia-Vidal, H J Lezec, K M Pellerin, T Thio, J B Pendry, and T W Ebbesen. Theory of extraordinary optical transmission through subwavelength hole arrays. *Phys. Rev. Lett.*, 86(6):1114, 2001.

[22] E Altewischer, M P Van Exter, and J P Woerdman. Plasmon-assisted transmission of entangled photons. *Nature*, 418(6895):304–306, 2002.

[23] Esteban Moreno, F J Garcia-Vidal, Daniel Erni, J Ignacio Cirac, and L Martín-Moreno. Theory of plasmon-assisted transmission of entangled photons. *Phys. Rev. Lett.*, 92(23):236801, 2004.

[24] Sylvain Fasel, Franck Robin, Esteban Moreno, Daniel Erni, Nicolas Gisin, and Hugo Zbinden. Energy-time entanglement preservation in plasmon-assisted light transmission. *Phys. Rev. Lett.*,

94(11):110501, 2005.

[25] Xi-Feng Ren, Guo-Ping Guo, Yun-Feng Huang, Chuan-Feng Li, and Guang-Can Guo. Plasmon-assisted transmission of high-dimensional orbital angular-momentum entangled state. *EPL (Europhysics Lett.*, 76(5):753, 2006.

[26] L. Olislager, J. Cussey, A. T. Nguyen, P. Emplit, S. Massar, J.-M. Merolla, and K. Phan Huy. Frequency-bin entangled photons. *Phys. Rev. A*, 82(1):013804, July 2010.

[27] Laurent Olislager, Ismaël Mbodji, Erik Woodhead, Johann Cussey, Luca Furfaro, Philippe Emplit, Serge Massar, Kien Phan Huy, and Jean-Marc Merolla. Implementing two-photon interference in the frequency domain with electro-optic phase modulators. *New J. Phys.*, 14(4):43015, 2012.

[28] Laurent Olislager, Erik Woodhead, Kien Phan Huy, Jean-Marc Merolla, Philippe Emplit, and Serge Massar. Creating and manipulating entangled optical qubits in the frequency domain. *Phys. Rev. A*, 89(5):52323, 2014.

[29] Simona Ungureanu, Branko Kolaric, Jianing Chen, Rainer Hillenbrand, and Renaud A L Vallée. Far-field disentanglement of modes in hybrid plasmonic-photonic crystals by fluorescence nano-reporters. *Nanophotonics*, 2(3):173–185, 2013.

[30] Pierre Fauché, Simona Ungureanu, Branko Kolaric, and Renaud A L Vallée. Emitters as probes of a complex plasmo-photonics mode. *J. Mater. Chem. C*, 2014.

[31] Shigenori Fujikawa, Rie Takaki, and Toyoki Kunitake. Fabrication of arrays of sub-20-nm silica walls via photolithography and solution-based molecular coating. *Langmuir*, 22(21):9057–61, October 2006.

[32] Wakana Kubo and Shigenori Fujikawa. Embedding of a gold nanofin array in a polymer film to create transparent, flexible and anisotropic electrodes. *J. Mater. Chem.*, 19(15):2154, March 2009.

[33] Wakana Kubo and Shigenori Fujikawa. Au double nanopillars with nanogap for plasmonic sensor. *Nano Lett.*, 11(1):8–15, January 2011.

[34] A. Taflove, A. Oskooi, and S. G. Johnson, editors. *Advances in FDTD Computational Electrodynamics: Photonics and Nanotechnology*. Artech House, Inc.„ 2013.

[35] A D Rakic, A B Djurišic, J M Elazar, and M L Majewski. Optical Properties of Metallic Films for Vertical-Cavity Optoelectronic Devices. *Appl. Opt.*, 37(22):5271–5283, August 1998.